Lab on a Chip

PAPER

View Article Online
View Journal | View Issue





Cite this: *Lab Chip*, 2020, **20**, 834

# Enrichment of rare events using a multi-parameter high throughput microfluidic droplet sorter†

Sheng-Ting Hung, [a] Srijit Mukherjee [ab] and Ralph Jimenez *[ab]

Received 9th August 2019,
Accepted 17th January 2020

DOI: 10.1039/c9lc00790c

rsc.li/loc

High information content analysis, enrichment, and selection of rare events from a large population are of great importance in biological and biomedical research. The fluorescence lifetime of a fluorophore, a photophysical property which is independent of and complementary to fluorescence intensity, has been incorporated into various imaging and sensing techniques through microscopy, flow cytometry and droplet microfluidics. However, the throughput of fluorescence lifetime activated droplet sorting is orders of magnitude lower than that of fluorescence activated cell sorting, making it unattractive for applications such as directed evolution of enzymes, despite its highly effective compartmentalization of library members. We developed a microfluidic sorter capable of selecting fluorophores based on fluorescence lifetime and brightness at two excitation and emission colors at a maximum droplet rate of 2.5 kHz. We also present a novel selection strategy for efficiently analyzing and/or enriching rare fluorescent members from a large population which capitalizes on the Poisson distribution of analyte encapsulation into droplets. The effectiveness of the droplet sorter and the new selection strategy are demonstrated by enriching rare populations from a ~$10^8$-member site-directed mutagenesis library of fluorescent proteins expressed in bacteria. This selection strategy can in principle be employed on many droplet sorting platforms, and thus can potentially impact broad areas of science where analysis and enrichment of rare events is needed.

## Introduction

Fluorescence lifetime is an intrinsic molecular property that is independent of excitation and emission intensity, local fluorophore concentration, and can be detected even with spectral overlaps among fluorophores and in the presence of cellular auto-fluorescence. Fluorophore lifetime is often sensitive to the solvent and biochemical environment, so it has been used as a detection parameter in imaging and sensing techniques.[1–4] In particular, fluorescence lifetime imaging microscopy (FLIM) is a powerful tool complementing fluorescence brightness-based imaging methods. It has been applied to subcellular pH measurements,[5,6] intracellular refractive index sensing,[7,8] molecular interactions in cells,[9–11] drug evaluation and discovery,[12–14] drug delivery and cancer studies.[15–18] Nonetheless, FLIM applications are hampered by its throughput. Flow cytometry incorporating fluorescence lifetime measurements could significantly improve the throughput, advancing applications to biological and biomedical research such as directed evolution of fluorescent proteins (FPs),[19] protein subcellular localization,[20] protein–protein interaction,[21] drug discovery,[22] and cellular physiology.[23,24]

Lifetime-based flow cytometry has been demonstrated at a sorting throughput of hundreds of cells per second.[25] However, there are limitations associated with fluorescence detection in a continuous flow stream. For cellular applications, it restricts the fluorescent markers and reactions to be inside or on the cellular surface and is limited to applications that are insensitive to inter-cellular interactions. One approach for overcoming these limitations is to encapsulate cells or other analytes into isolated droplets that retain their integrity throughout the analysis, and sorting. The ease with which stable droplets can be formed with pL-scale, tunable volumes makes droplet microfluidics particularly useful for analyzing individual molecules, cells or other discrete analytes such as beads. These capabilities has been utilized for studying enzymatic activity *in cellulo*[26,27] and *in vitro*,[28] single-cell analysis and sorting,[29] screening for antibiotic resistance,[30,31] directed evolution of enzymes,[32] genetically-encoded biosensors,[33,34] and quantifying heterogeneity at the single cell level.[35,36] Moreover, microfluidic droplet platforms can be designed for novel flow cytometry applications such as those simultaneously requiring temporally well-defined mixing of cells with reagents followed by time-resolved detection. Fiedler and coworkers have demonstrated resolution and sorting of

[a] *JILA, NIST and University of Colorado, Boulder, Colorado 80309, USA. E-mail: rjimenez@jila.colorado.edu*
[b] *Department of Chemistry, University of Colorado, Boulder, Colorado 80309, USA*
† Electronic supplementary information (ESI) available. See DOI: 10.1039/c9lc00790c

genetically-encoded biosensors based on various Förster resonance energy transfer (FRET) ratios measured with delay time in seconds.[34] The same platform can be readily modified for directed evolution of fluorescent proteins or enzymes.

The throughput of lifetime-based droplet sorters is impacted by a number of factors. First, the statistics of cell loading into droplets typically follows the Poisson distribution.[37] To ensure single cell loading, the proportion of non-empty droplets is often limited to <10% of the whole droplet population. Unfortunately, this sparse loading limits the throughput and is therefore often regarded as a disadvantage of the droplet platform. Deterministic single cell encapsulation methods overcome the limitation imposed by Poisson statistics, but there are other limitations such as increased device complexity, substantial proportion of unsorted or wrongly selected droplets, and high flow rates, which limit the flexibility of integration with other systems.[38] Second, the throughput of a conventional droplet sorter is limited to 2–3 kHz due to the use of a hard divider to separate the collection and waste channels, but new geometries have been investigated to surpass this limitation achieving brightness-based sorting at 30 kHz.[39] Finally, fast data processing of fluorescence lifetime signatures and real-time sorting decision and actuation components are crucial for achieving kHz sorting rates. Despite advances in incorporating fluorescence lifetime measurements into droplet selection methods, the throughput is much lower than purely brightness-based droplet sorting. For example, the throughput of a recently reported fluorescence lifetime droplet microfluidic sorter is 50 droplets per s.[40] A FACS enrichment step is often used to enrich a subset of targets from a large pool prior to selection or investigation on other parameters and platforms.[19,41–43] Performing fluorescence lifetime selection with this combination of methods is disadvantageous. In addition to the restrictions imposed by a continuous flow stream in the FACS step, the use of two different instruments imposes uncertainties into the overall selection because the fluorescence intensity values are difficult to calibrate between instruments.

Within the general realm of sorting applications, the analysis, enrichment, and isolation of rare macromolecules, cells and particles from a large population constitutes an important subset that is of great importance across a broad area of biomedical, biotechnological, and environmental science. Several papers have described approaches to this challenge in which a rare population is analyzed without isolating it, or where an initial enrichment is advantageous compared to one-step, single-particle isolation. For example, fluorescence brightness-based droplet digital detection has been applied to the detection of single bacteria in unprocessed blood[44] and profiling circulating tumor DNA,[45] and the implementation of fluorescence lifetime detection was demonstrated to increase the specificity of particle counting.[46] An ensemble sorting approach which repeatedly analyzes and sorts batches within a sample was recently proposed for enriching or separate fluorescent particles.[47] Many microfluidic systems have been developed to enrich and isolate circulating tumor cells, as reviewed in ref. 48. Here, we quantify the advantages of a batch sorting technique for increasing the throughput of rare-clone isolation.

In this work, we have developed a multiparameter high throughput water in oil droplet microfluidic sorter capable of screening and sorting analytes based on emission spectra, emission brightness, and fluorescence lifetime. We raised the throughput of lifetime sorting to the upper limit possible for a droplet sorter with a hard divider between collection and waste channels.[39] This performance constitutes a 50-fold increase compared to a recently reported lifetime droplet sorter.[40] We also describe and demonstrate a novel selection strategy, similar to an ensemble-based approach, which exploits the Poisson statistics of analytes in droplets overloaded with multiple analytes. This method provides a several-fold enhancement in sorting throughput. The strategy can be used to analyze and enrich rare events from a large population in either a qualitative manner without prior knowledge for the initial frequency of the rare events, or in a quantitative fashion with controls of the efficiency and precision of enrichment when the initial frequency of the rare events is estimated. The enriched sub-population can be subjected to further multiparameter analysis and selection with single-cell resolution on the same microfluidic platform. We demonstrate the power of this multiparameter droplet sorter and the enrichment strategy in the context of directed evolution of red fluorescent proteins (RFPs) expressed in *E. coli*.

# Experimental

### Optical layout

The optical layout of the instrument is depicted in section S1 of ESI.† Both 561 nm and 450 nm continuous wave (CW) laser beams excite fluorescence from the cells encapsulated in droplets. The 561 nm beam is focused into an electro-optic modulator that can amplitude modulate the CW beam to a sinusoidal profile. The red and green fluorescence signals are separated by a dichroic mirror and detected by photomultiplier tubes (PMTs).

### Electronics and microfluidic device

The main improvement of sorting throughput in this work is due to the implementation of faster electronics. The layout of the detection electronics is schematically described in Fig. 1. The electro-optic modulator (EOM; ThorLabs EO-AM-NR-C4) is used to modulate the 561 nm laser light and is driven using a function generator (Agilent 33520B) that provides a 1 V peak to peak sinusoidal signal at 29.5 MHz to a resonator circuit. When screening or sorting based on fluorescence lifetime, the red fluorescence signals from PMT1 are separated into a radio frequency (RF) component (that bears the lifetime information) and the direct current (DC, <83 kHz) component using a bias tee. To improve the signal to

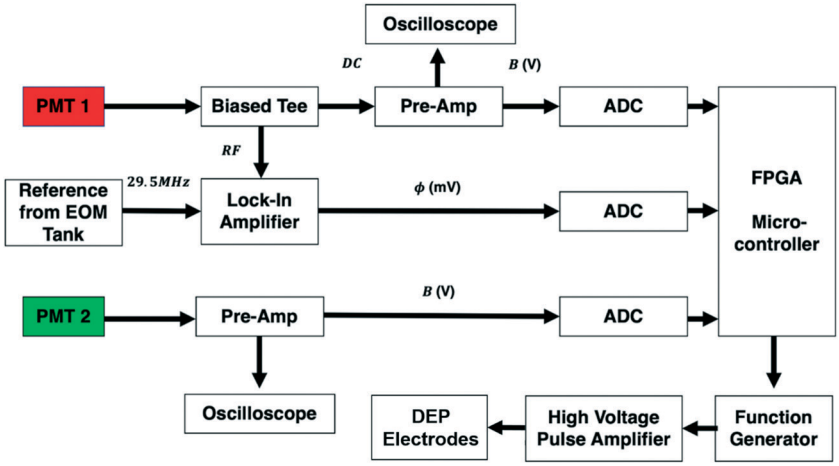


**Fig. 1** Schematic layout of the electronics used in this sorter.

noise ratio, the DC signals from the biased-tee and from PMT2 (green fluorescence) are amplified using home-built trans-impedance log or linear pre-amplifiers, depending upon the experiment and sample in use,[19] then digitized using analog to digital converter (ADC) boards (Analog Devices, EVAL-AD7986FMCZ, 18 bit). The RF component of the signal is passed onto a commercial high-speed lock-in amplifier (Zurich Instruments UHFLI), which calculates the phase shift of the fluorescence signal relative to the sinusoidal modulation signal to extract information of fluorescence lifetime. The phase shift value from the lock-in amplifier is then digitized using the same type of ADC boards employed for brightness measurements. The digitized signals from the boards are then fed into a customized field programmable gate array (FPGA) board that makes decisions based on user defined parameters interfaced through a LabView program. Use of an FPGA has been demonstrated to enhance the data processing rate for fluorescence lifetime calculation.[49] Brightness and lifetime signals from encapsulated cells in droplets that fulfil the selection criteria are then sorted using dielectrophoresis (DEP) technique.[34] The FPGA sends a sort signal to trigger a function generator (Keysight 33509B) which provides a square wave pulse which is amplified 1000× in a high voltage amplifier (TREK), before being sent to the electrodes of the microfluidic device. The flow is biased towards the waste channel, so droplets are only directed to the collection channel when the FPGA sends a signal to trigger a high voltage pulse to DEP electrodes. The fluorescence detection and cell selection regions of the device are shown in Fig. 2(a). Further details on the microfluidic device are provided in section S1 of ESI.†

## Instrument operation

The microfluidic sorter is configured with excitation beams at 450 nm and 561 nm, wavelengths which allow for screening based on green and/or red fluorescence signals respectively. The 561 nm excitation beam is modulated at 29.5 MHz, enabling fluorescence lifetime screening in the red channel. To count the number of droplets passing each channel and monitor the flow (number of droplets per second) throughout an experiment, the laser intensities and PMT voltages were set such that a small portion of scattered laser light from each droplet bleeds through the dichroic

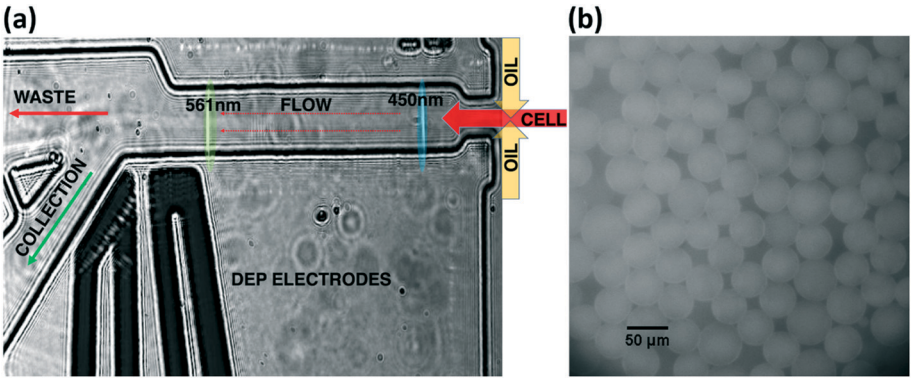


**Fig. 2** (a) Camera image shows the typical droplet flow with both excitation beams on. The microfluidic chip is designed such that droplets are biased towards the waste channel. (b) Image of droplets containing rhodamine B generated with the microfluidic chip. The scale bar indicates 50 μm.

 

mirror and the emission filters and can be detected in both channels. We previously reported fluorescence lifetime sorting in a microfluidic flow cytometer, however, the sorting speed was limited to ~30 cells per s because communication among instruments, target and host computers, calculation of fluorescence phase shifts, and sorting decisions relied on software developed on a LabView platform.[19] In the current sorter, the phase shifts are obtained directly from a high-speed lock-in amplifier, and an FPGA coordinates communication among all electronics and performs sorting decisions. A LabView user interface is designed only for setting selection parameters, acquiring data from the FPGA and real time plotting. As a result, the new instrument operates at ~100-fold higher screening and sorting speeds. For both fluorescence-activated droplet sorting ("brightness sorting") and fluorescence lifetime-activated droplet sorting ("lifetime sorting"), the FPGA and Labview program are designed such that the sorting thresholds can be set to exclude empty and unwanted droplets for sorting purposes, while counting the total number of droplets and monitoring the flow (number of droplets per second). Both brightness and lifetime measurements have been tested at droplet generation rates up to 4 KHz (~0.7 mL $h^{-1}$ volumetric flow rate) for screening and 2.5 kHz (~0.45 mL $h^{-1}$ volumetric flow rate) for sorting. A typical image of droplets generated at ~2.5 kHz (Fig. 2(b)), demonstrates their size uniformity and agreement with the estimated droplet volume ~50 pL which is determined from the droplet generation rate and the 0.45 mL $h^{-1}$ volumetric flow rate. More details about instrument operation are supplied in section S2 of the ESI.†

### Cell culture and sample preparation

The droplet microfluidic sorter can be employed to assay diverse cell types, such as bacteria, phytoplankton, yeast, and mammalian cell lines. To test the performance of this sorter, various FPs with distinct fluorescence lifetime, brightness, and spectra were expressed in *E. coli*. Cells expressing FPs were prepared at desired concentrations according to the measurement of their optical density (OD) and connected to the aqueous inlet of the microfluidic chip. The details of cell culture and sample preparation are described in section S3 of ESI.†

## Results and discussion

This instrument control software is designed such that one can choose the desired combinations of screening and/or sorting based on emission spectrum, brightness, and red fluorescence lifetime. The scattered excitation light from each droplet can be detected by the PMTs, which allows us to monitor the flow, count the number of droplets, and pair-match two events in green and red channels for a particular droplet. Details of data acquisition and signal processing are described in section S4 of ESI.† The performance of brightness and lifetime sorting with different screening/sorting criteria is evaluated here. We also present some examples of the strategy for enriching rare events with multiple cell encapsulation.

### Performance of two-color brightness-sorting

To evaluate the performance of brightness detection in the green and red channels, *E. coli* cells expressing EGFP and mScarlet were screened respectively to find the mean brightness in each channel. An approximately 1 : 1 mixture was prepared and droplets with a brightness threshold greater than mean brightness in the red channel were sorted to select mScarlet from ~$10^5$ droplets. The sorted cells were subsequently grown overnight and screened 16 hours after induction of expression to evaluate the sorting efficiency. All screening and sorting experiments were performed at a rate of 2 kHz with an average cell concentration of 0.1 cell per droplet, where 9.5% of the droplets are filled and 95% of filled droplets contain a single cell. The results shown in section S5 of ESI† reveal a sorting efficiency of 86 ± 1% averaged from 3 experimental trials, *i.e.* 86% of re-grown cells have mScarlet and 14% of them have EGFP in average. The 14% re-grown cells expressing EGFP reflects several factors including the 5% of filled droplets containing multiple cells, varying cytotoxicity for cells expressing different FPs,[50] and the excitation conditions. These issues are discussed in the lifetime sorting section, below.

### Performance of lifetime sorting

The phase shift measured in the frequency domain technique is sensitive to the modulation frequency,[51] transit time of cells passing through the laser beam, and settings of the PMT and lock-in amplifier. Determination of the lifetime and its dependence on these experimental factors is described in section S4 of ESI.† *E. coli* cells expressing mCherry, mApple, or mScarlet were screened with brightness and lifetime at a rate of 2.5 kHz. The major population of each RFP is distinguishable by its fluorescence lifetime as shown in Fig. 3(a). The results reveal heterogeneity in both fluorescence brightness and lifetime, as observed in our previous work on other RFPs.[19] The spread of lifetime values is about 0.5–1 ns for these RFPs at full width at half maximum (FWHM) of the histograms in Fig. 3(b).

The asymmetric histograms of fluorescence lifetime in Fig. 3(b) can be understood as an effect resulting from the contribution of scattered excitation light detected along with the fluorescence signal. This effect is modeled with a simulation in section S4 of the ESI.† Ideally, scattered light has a constant phase shift (which is converted to the fluorescence lifetime) relative to the modulated laser beam due to optical and electronic delays. This is included in the total phase shift by setting the reference phase shift of a bacterial colony expressing mCherry on a plate to 45 degrees. In this particular experiment, the total offset phase shift of empty droplets corresponds to a fluorescence lifetime centered on ~2.35 ns with a wide distribution due to low signal-to-noise ratio (SNR). The scattered light is added to the

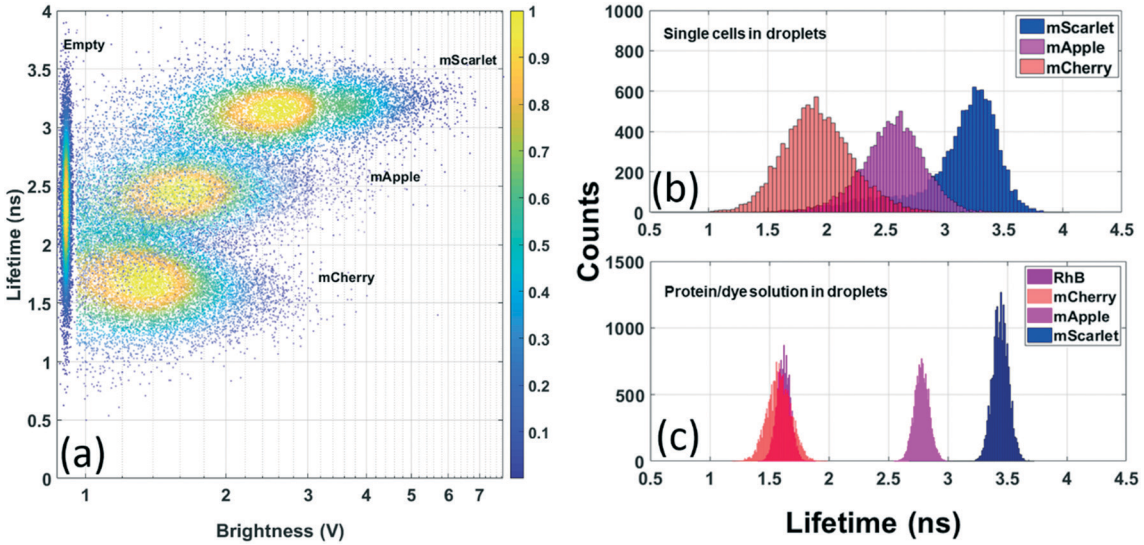


**Fig. 3** (a) Fluorescence lifetime and brightness plots of empty droplets and individual RFPs expressed in *E. coli* screened sequentially ($10^4$ cells each). Pseudocolor indicates the normalized cell counts with a particular bin of fluorescence lifetime and brightness on the plot, ranging from yellow for the highest to indigo indicating the lowest counts. The mean fluorescence lifetime is 1.7 ns (set as reference), 2.6 ns, and 3.3 ns for mCherry, mApple, and mScarlet respectively. (b) Corresponding fluorescence lifetime histograms. (c) Fluorescence lifetime histograms of rhodamine B (RhB) and three purified proteins measured in the microfluidic sorter. The mean fluorescence lifetime is 1.6 ns (set as reference), 1.6 ns, 2.8 ns, and 3.5 ns for RhB, mCherry, mApple, and mScarlet respectively.

fluorescence signal and both signals have the same modulation frequency but different phase shift values, so the lock-in amplifier extracts an averaged phase value from the combined signals. The influence of scattered light is more significant at low fluorescence brightness, whereas the average lifetime value approaches the actual fluorescence lifetime value as the fluorescence brightness increases.

The distribution of lifetime measured from a single-FP population can be attributed to cellular heterogeneity, excitation condition and electronics. Cellular heterogeneity is an intrinsic biochemical property that can only be resolved in single cell analysis methods such as this microfluidic droplet sorter. On the other hand, the noise originating from the excitation condition may be further reduced. The diameter of the droplet is estimated to be ~46 μm, but the Rayleigh length of the excitation beam is ~10 μm, hence the location of the cell inside a droplet could lead to variations in fluorescence brightness resulting in uncertainties in lifetime measurement. Theoretically the lifetime is independent of fluorescence signal level, but in practice the scattered excitation light affects weaker fluorescence signals more than stronger ones as discussed above. We further investigated the spread of lifetime due to electronics by performing *in vitro* measurements. In addition to eliminating the cellular heterogeneity, *in vitro* measurements also minimize the fluctuations from excitation condition since a droplet has homogeneous fluorophore concentration and the Rayleigh length is always within the droplet. It is worth noting that various *in vitro* assays can be performed with a droplet platform, but it is difficult to perform them with a continuous stream cytometry. Three purified proteins, mCherry, mApple, and mScarlet, and an organic dye, rhodamine B, were screened for fluorescence lifetime using the sorter. The histogram of fluorescence lifetime is shown in Fig. 3(c), with FWHM ~0.1 ns for rhodamine B and ~0.2–0.3 ns for FPs. The wide spread in lifetime for mCherry is likely due to its low SNR resulting from a low quantum yield (hence low molecular brightness). Nonetheless, the FWHM of fluorescence lifetime measured from an *in vitro* experiment is much narrower than that from a cellular measurement. The result indicates that the uncertainty originating from electronics is significantly less than other sources. This also suggests that the lifetime resolution for cellular screening could be improved by reducing the droplet size and/or expanding the beam size to extend the Rayleigh length to ensure that the encapsulated cells are within the Rayleigh length, *i.e.* an improved uniform excitation condition. This effect will be reduced with larger cell types such as yeast or mammalian cells. Finally, note that the disagreement in the average lifetime among cellular and *in vitro* measurements suggests that the cellular environment differs from the *in vitro* environment. For example, fluorescence lifetime of FPs varying with environmental pH[5,6] and refractive index[7,8] has been reported and used for sensing and imaging applications. Details of the *in vitro* experiment including the comparison of fluorescence lifetime measured using the sorter and time-correlated single photon counting (TCSPC) are described in section S5 of ESI.†

To demonstrate the performance of lifetime-based sorting, *E. coli* cells expressing mScarlet or mCherry were mixed in a ~1 : 1 proportion and sorted at 2.5 kHz with two parameters, fluorescence lifetime and brightness, at an average concentration of 0.1 cell per droplet. This sort rate represents the fastest fluorescence lifetime droplet sorting reported to

 

date. Approximately $3 \times 10^3$ droplets were sorted from ~$2.5 \times 10^5$ droplets with the selection gates set to the mean brightness value and mean fluorescence lifetime of mScarlet. The sorted cells were subsequently grown, expressed for 16 hours and re-screened to evaluate the sorting efficiency. The screening results before and after sorting are shown in Fig. 4, demonstrating an 85% sorting efficiency. The experiment was additionally repeated 3 times with a new mixture, sorting mScarlet or mCherry, and the average efficiencies were 80 ± 1% and 97 ± 1% respectively, as described in section S5 of ESI.† The discrepancy between sorting mScarlet and mCherry can be attributed to the process of re-growing and expressing enriched cells in the experiment with the assumption that bacteria expressing different FPs have the same growth rate, which may not be accurate. Some mCherry mutants, mApple, and EGFP have been reported to show a range of cytotoxicities when expressed in *E. coli*.[50] The difference between two batches of mScarlet enrichment experiments may be due to the flow condition, the biological variation (two biological duplicates in two batches of experiments) and the uncertainty of cell concentration in the sample preparation causing variations in average number of cells per droplet ($\lambda$), which affects the sorting efficiency that will be further discussed below.

### Strategy for enriching rare fluorescent events

For a large library containing rare events, the overall sorting throughput can be greatly increased by encapsulating multiple cells in a single droplet as an initial round of enrichment. The efficiency of this strategy can be estimated by considering the Poisson distribution, the combination of cells resulting fluorescent droplets, and the percentages of fluorescent cells in a library. The combination of cells encapsulated in droplets is illustrated in the inset of Fig. 5. A droplet will be detected with fluorescence as long as it contains one or more fluorescent cells. The probability of number of cells ($N$) encapsulated in a droplet is Prob($N$) = $(e^{-\lambda} \times \lambda^N)/N!$, where $\lambda$ is the average number of cells per droplet.

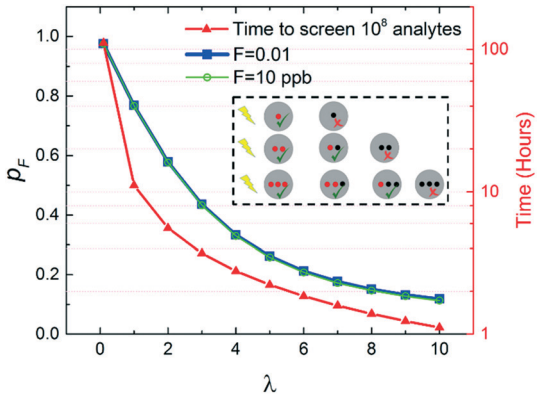


Fig. 5 The efficiency of enrichment with various initial fraction of target analyte (cells, molecules, or beads) and the required enrichment time as a function of average number of cells per droplet. Inset (dashed box): Illustration of cells encapsulated in droplets. The red and black dots indicate fluorescent and non-fluorescent cells, respectively. The green check and red cross marks indicate fluorescent and non-fluorescent droplets.

Assuming a library with initial fraction $F$ of fluorescent cells, the probability of finding fluorescent cells after sorting, $p_F$, is

$$p_F = \sum_{n=1}^{\infty} \frac{\sum_{i=1}^{n} \binom{n}{i} \cdot i \cdot F^i \cdot (1-F)^{n-1}}{n \cdot \sum_{i=1}^{n} \binom{n}{i} \cdot F^i \cdot (1-F)^{n-1}},$$

where $i$ is the number of fluorescent cells and $n$ is the number of cells per droplet. Since the probability of encapsulated cells

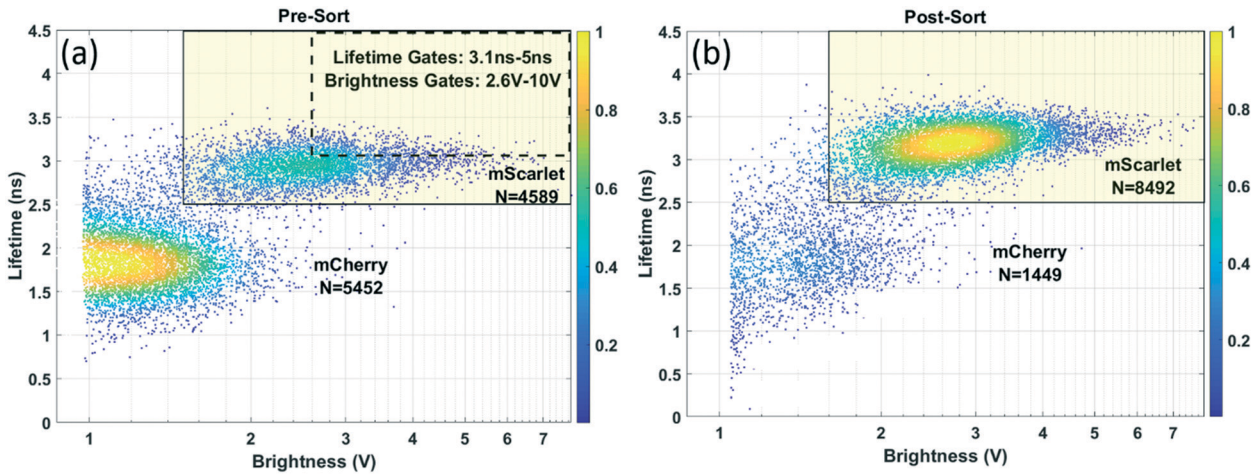


Fig. 4 Fluorescence lifetime *versus* brightness scatter plots of mixed cells before and after sorting. Solid boxes indicate the thresholds for counting cells expressing mScarlet. $N$ is the number of cells expressing each RFP. (a) Mixture of *E. coli* cells expressing mCherry and mScarlet before sorting. The dashed box indicates the two-parameter sorting gates. (b) Screening results after sorted cells were grown overnight and expressed for 16 hours. The brightness threshold was set slightly higher than pre-sort to exclude the stronger scattered excitation signals from droplets in the post-sort screening, because changing microfluidic chips introduces variations in the focus of the excitation beam and thus the amount of scattered light.

per droplet decreases quickly with the increasing number of encapsulated cells, the $p_F$ can be numerically calculated using $n \leq 50$ for $\lambda \leq 10$. The Poisson distribution for $\lambda \leq 10$ is plotted in section S6 of ESI.† The efficiency of the multiple-cell encapsulation enrichment, which is indicated by the improvement in the fraction of fluorescent cells after sorting (*i.e.* $p_F$), is estimated with $F = 0.01$ and $F = 10$ ppb for various $\lambda$ as shown in Fig. 5. The results indicate that with one round of sorting, the fluorescent cells in the library can be enriched to about the same fraction regardless of the initial fraction $F$, thus this selection strategy is more powerful for enriching rarer events from a large pool (*i.e.* small $F$). It is not surprising that the enrichment efficiency is significantly affected by the average number of cells per droplet ($\lambda$), but the influence from the fraction of fluorescent cells in the original library is not significant, because the selected droplets all contain fluorescent cells. Assuming a sorting speed of 2.5 kHz, the time required for screening $10^8$ cells as a function of $\lambda$ is plotted in Fig. 5. The result clearly shows that the time can be drastically reduced by including multiple cells in a droplet. The estimation of $p_F$ only considers the statistical probability, *i.e.* the number of screened cells is much larger than the inverse of the initial fraction $F$. Such enrichment efficiency, $p_F$, is estimated to hold for enriching ≥0.5 ppm targets from $10^8$ cells, the limit for current throughput to complete enrichment in a few hours without losing cell viability, in section S6 of ESI.† However, this does not limit the application of the enrichment strategy from sorting smaller fraction of rare events. With smaller fraction of rare events, the enrichment efficiency may deviate from the expected value plotted in Fig. 5, but it still provides approximately the same order of magnitude of enrichment efficiency as illustrated in section S6 of ESI.†

To further illustrate the power of this enrichment strategy, we consider two examples of rare events that fluoresce or exhibit a distinct fluorescence lifetime relative to the main fluorescent population. Assume the enrichment is carried out with brightness or lifetime sorting operating at 2.5 kHz with an average 4 cells per droplet encapsulation. In the first example, we assume that the fraction of the rare events is 1 ppm. It would take less than 3 hours to enrich rare events from a $10^8$ population, resulting in a subset of 100 fluorescent cells mixed with 203 unwanted cells ($p_F = 0.33$), *i.e.* $3.3 \times 10^5$-fold enrichment ($p_F/F$) in one round of sorting. The enriched subset can be further cultured, analyzed, or sorted with single cell resolution to isolate the final, purified population. In the second example, we consider a cell-based library containing $33 \times 10^6$ distinct mutants. To ensure the enrichment covers 95% of this library, at least 3 times of the library size must be screened,[52] which is $\sim 10^8$ cells. Assuming the desired clones comprise 1% of the original library, this enrichment reduces the library size from $33 \times 10^6$ down to $1 \times 10^6$ within 3 hours with $0.33 \times 10^6$ fluorescent cells, thus a 33-fold enrichment. The enriched library can be further analyzed or sorted at $\lambda = 0.1$ (single-cell resolution) using brightness or lifetime sorting. Using the conventional encapsulation strategy ($\lambda = 0.1$) without the enrichment, it would take ~117 hours to complete the selection in both examples with brightness or lifetime sorting at the speed of 2.5 kHz developed in this work. It would take 50 times longer (~5848 hours) for a recently reported lifetime droplet sorting[40] to perform the selection. Using a state-of-the-art droplet sorting at 30 kHz,[39] the selection would require ~10 hours, which is more than 3 times longer than the lifetime enrichment demonstrated here, to complete a brightness-only selection in single cell resolution without fluorescence lifetime information. The combination of this new sorting technology and enrichment strategy enables fast multiparameter analysis and selection of rare events from a $10^8$-member population based on fluorescence lifetime, brightness, and spectrum, as a preparation for further investigation and sorting with single cell resolution on a single instrument.

To demonstrate the effectiveness of this strategy, we enriched mScarlet from a mixture of EGFP and mScarlet transformed in *E. coli* using dual color brightness sorting. Since EGFP does not emit red fluorescence, EGFP can be regarded as the non-fluorescent population and mScarlet as the rare fluorescent population observed in the red channel. The number of EGFP cells can be counted in the green channel since only EGFP contributes to the green emission. Thus, the fraction of mScarlet (*i.e.* the fluorescent events in the red channel) in the mixture was determined to be $F \sim 0.01$. After one round of enrichment with $\lambda = 3$ encapsulation, the sorted cells were subsequently grown, expressed and screened with $\lambda \leq 0.1$ encapsulation. The mScarlet population was enriched to an average 35 ± 4%, which agrees with the expected value ($p_F \times 0.86$) ~37%, taking into account the 86% efficiency of single cell two-color sorting described earlier. The experimental details can be found in section S6 of ESI.†

The enrichment strategy can also be applied in lifetime sorting when the rare events have a distinct fluorescence lifetime from the major population, despite the overlap in emission spectra and brightness. We demonstrate the enrichment of rare cells expressed with mScarlet from a mixture of mCherry and mScarlet, which have large overlap in both emission spectra and cellular brightness. The first test was carried out the same day using the same batch of sample generating results in Fig. 4. The fraction of mScarlet in the mixture before enrichment was estimated to be $F \sim 5 \times 10^{-3}$. The enrichment was performed with $\lambda = 3$ at 2.5 kHz, and the sorted cells were subsequently grown, expressed and screened with $\lambda \leq 0.1$. We attained an enrichment of the mScarlet population to 40% (Fig. 6), which is consistent with the expected value, including the 85% efficiency of single cell lifetime sorting demonstrated in Fig. 4, ($p_F \times 0.85$) ~37%. Another enrichment for rare mScarlet was performed using the second batch of sample with $F \sim 5 \times 10^{-3}$, resulting in an average enrichment of the mScarlet population 30 ± 5%, in agreement with the expectation ($p_F \times 0.80$) ~35%. Experimental details are described in section S6 of ESI.†

 

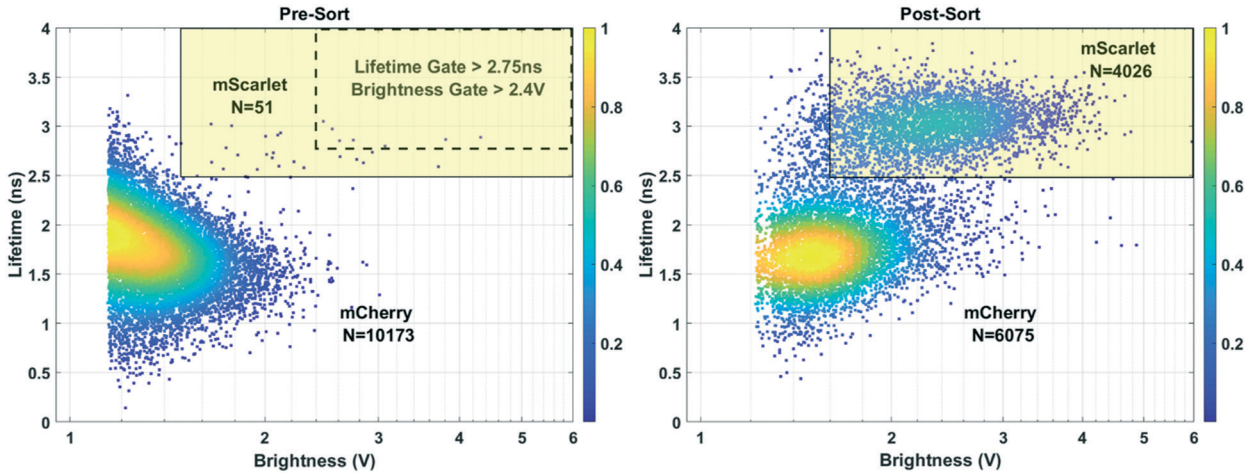


**Fig. 6** Fluorescence lifetime *versus* brightness scatter plots of rare mScarlet enrichment. Solid boxes illustrate thresholds for counting cells expressing mScarlet. *N* is the number of cells expressing each RFP. (Left) Mixture of *E. coli* cells expressing mCherry and mScarlet before enrichment. The dashed box indicates the two-parameter sorting gates. (Right) Screening results after enriched cells were grown overnight and expressed for 16 hours.

### Enrichment of an RFP library

The directed evolution of FPs often involves the screening of cell libraries with rare bright clones. Library size increases exponentially with the number of target residues, and FP libraries are typically found to have a narrow fitness landscape,[53] *i.e.* the fraction of fluorescent clones dramatically decreases as the mutational space increases due to protein mis-folding, incomplete chromophore maturation, and other photophysical factors. We used this sorter to enrich the population of fluorescent RFP mutants and select the brightest ones for further development. Taking mScarlet-I as the template, we constructed a site-directed library with the size $\sim 1.7 \times 10^7$, which requires screening $>5.1 \times 10^7$ cells to cover 95% of the library size. In our previous studies of site-directed and/or error-prone PCR libraries of RFPs, some non-fluorescent colonies were observed to grow larger than fluorescent ones on plates, likely due to variations in cytotoxicity of various mutations in RFPs.[50] Therefore, we expect reduced sorting efficiency due to the re-growth and expression processes after enrichment as described above. With this consideration in mind, we decided to load the droplets with $\lambda = 3$, and a total number of $\sim 8 \times 10^7$ *E. coli* cells expressing this RFP library was screened in two batches (ensuring the health of cells) to enrich fluorescent cells at ~2 kHz. The proportion of fluorescent cells was enriched from initially ~5% to ~30%. This is lower than the expected, empirically corrected enrichment efficiency (43% × 0.86) 37% for $\lambda = 3$. The enriched population underwent 3 more rounds of enrichments with higher thresholds in fluorescent brightness with $\lambda = 1$ or $\lambda = 0.1$ at 2 kHz, resulting in >95% fluorescent population. The final round of sorted cells was re-grown overnight then expressed on agar plates. Three distinct mutants were identified from the agar plates for further development. More information on the library and the detailed enrichment procedure are provided in section S7 of ESI.†

This platform is sufficiently flexible to support further enhancements. For example, additional excitation wavelengths with RF modulation can be implemented to expand the information content in both spectral and fluorescence lifetime dimensions. Furthermore, it is possible to increase the sorting speed further by modifying the microfluidic chip design. In particular, brightness sorting at 30 kHz has been demonstrated in a design where the hard divider is replaced with a gapped divider to separate outlets.[39] In addition, increasing the modulation frequency of the excitation beam shortens the phase acquisition time, and therefore increases the fluorescence lifetime detection speed. As such, a modulation frequency of 100 MHz could support a ~3.4-fold increase in sorting speed. However, the modulation frequency may set the limit for the throughput of fluorescence lifetime measurement. When the modulation frequency increases to higher than 100 MHz, the period of the modulation wave becomes less than 10 ns, the same order of magnitude as the fluorescence lifetime of commonly used fluorophores. This may disturb the phase measurement under a strong excitation rate used in frequency domain measurement. On the other hand, to further increase the sorting speed to ≥10 kHz, the adjoining scattering or fluorescence signals are ≤100 μs apart. In current setup, the FWHM of the scattering and fluorescence signals is approximately 25 μs at 2 kHz, which is sufficiently small for sorting at 10 kHz. If needed, decreasing the droplet size can not only reduce the noise as previously discussed, but also shorten the transient time of the droplet and cells since they only pass the Rayleigh length region, resulting in narrower FWHM of the scattering and fluorescence signals. Thus, it is feasible to improve the throughput of this multiparameter droplet sorter to ≥10 kHz.

## Conclusion

A multiparameter microfluidic droplet sorter combining the detection of fluorescence lifetime, brightness, and spectrum has been developed in this work. The throughput of the fluorescence lifetime measurement and sorting, up to 4 kHz for screening and 2.5 kHz for sorting with current chip design, is greatly enhanced by using a FPGA for the communication among all electronics and sorting decisions. To our knowledge, this is the fastest fluorescence lifetime droplet screening and sorting speed to date. The high-throughput fluorescence lifetime droplet sorting opens the opportunity of integrating fluorescence lifetime detection with other high throughput detection methods in a microfluidic droplet platform to increase the information content of biological and biomedical assays with single cell resolution.

We have also proposed a novel multiple-cell encapsulation strategy enriching the rare events to overcome the obstacle of droplet sorting throughput limited by the nature of Poisson distribution for random cell/molecule encapsulation – by taking the advantage of Poisson statistics. The effect of enrichment increases tremendously as the fraction of rare events decreases. The efficiency and precision of enrichment can be quantitatively controlled if the rare event frequency is estimated before sorting. The enrichment strategy has been demonstrated to be effective in both brightness and lifetime sorting. Combining the enrichment strategy and the multiparameter microfluidic platform allows one to analyze and enrich rare events from a population $>10^8$ within a few hours. Though the enrichment does not provide single cell/analyte resolution, it greatly reduces the time required to search for rare events, thus is an efficient way to analyze or prepare rare events for further investigation or selection with single cell/analyte resolution. It is also feasible to improve the throughput of the multiparameter sorting to $\geq$10 kHz. Together with the new sorting strategy, the speed of droplet-encapsulated rare events analysis and enrichment can potentially exceed FACS, achieving an unprecedented throughput for microfluidics-based cell sorting.

## Conflicts of interest

There are no conflicts to declare.

## Acknowledgements

S. M. was supported by the NIH/CU Molecular Biophysics Training Program (T32). This work was supported by the NSF Physics Frontier Center at JILA (PHY 1734006 to R. J.) We acknowledge Dr. Nancy Douglas, Connor Thomas, and Annika Ekrem for assistance with cell culture, Dr. Felix Vietmeyer for valuable discussions in the implementation of electronics, and Prof. Amy Palmer and Dr. Premashis Manna for insightful discussions in the design of mScarlet-I library. R. J. is a staff member in the Quantum Physics Division of the National Institute of Standards and Technology (NIST). Certain commercial equipment, instruments, or materials are identified in this paper in order to specify the experimental procedure adequately. Such identification is not intended to imply recommendation or endorsement by the NIST, nor is it intended to imply that the materials or equipment identified are necessarily the best available for the purpose.

## References

1 N. Inada, N. Fukuda, T. Hayashi and S. Uchiyama, *Nat. Protoc.*, 2019, **14**, 1293.
2 P. H. Lakner, M. G. Monaghan, Y. Möller, M. A. Olayioye and K. Schenke-Layland, *Sci. Rep.*, 2017, **7**, 42730.
3 K. Suhling, L. M. Hirvonen, J. A. Levitt, P.-H. Chung, C. Tregidgo, A. Le Marois, D. A. Rusakov, K. Zheng, S. Ameer-Beg and S. Poland, others, *Med. Photon.*, 2015, **27**, 3–40.
4 C. A. Bücherl, A. Bader, A. H. Westphal, S. P. Laptenok and J. W. Borst, *Protoplasma*, 2014, **251**, 383–394.
5 M. Benvcina, *Sensors*, 2013, **13**, 16736–16758.
6 F.-J. Schmitt, B. Thaa, C. Junghans, M. Vitali, M. Veit and T. Friedrich, *Biochim. Biophys. Acta*, 2014, **1837**, 1581–1593.
7 H.-J. Van Manen, P. Verkuijlen, P. Wittendorp, V. Subramaniam, T. K. Van den Berg, D. Roos and C. Otto, *Biophys. J.*, 2008, **94**, L67–L69.
8 A. Pliss, X. Peng, L. Liu, A. Kuzmin, Y. Wang, J. Qu, Y. Li and P. N. Prasad, *Theranostics*, 2015, **5**, 919–930.
9 A. Margineanu, J. J. Chan, D. J. Kelly, S. C. Warren, D. Flatters, S. Kumar, M. Katan, C. W. Dunsby and P. M. French, *Sci. Rep.*, 2016, **6**, 28186.
10 R. T. Rebbeck, M. M. Essawy, F. R. Nitu, B. D. Grant, G. D. Gillispie, D. D. Thomas, D. M. Bers and R. L. Cornea, *SLAS Discovery*, 2017, **22**, 176–186.
11 Y. Long, Y. Stahl, S. Weidtkamp-Peters, M. Postma, W. Zhou, J. Goedhart, M.-I. Sánchez-Pérez, T. W. Gadella, R. Simon and B. Scheres, others, *Nature*, 2017, **548**, 97–102.
12 C. B. Talbot, J. McGinty, D. M. Grant, E. J. McGhee, D. M. Owen, W. Zhang, T. D. Bunney, I. Munro, B. Isherwood and R. Eagle, others, *J. Biophotonics*, 2008, **1**, 514–521.
13 S. Kawanabe, Y. Araki, T. Uchimura and T. Imasaka, *Methods Appl. Fluoresc.*, 2015, **3**, 025006.
14 J. Humpolívcková, J. Weber, J. Starková, E. Masínová, J. Günterová, I. Flaisigová, J. Konvalinka and T. Majerová, *Sci. Rep.*, 2018, **8**, 10438.
15 X. Dai, Z. Yue, M. E. Eccleston, J. Swartling, N. K. Slater and C. F. Kaminski, *Nanomedicine*, 2008, **4**, 49–56.
16 G.-J. Bakker, V. Andresen, R. M. Hoffman and P. Friedl, in *Methods in enzymology*, Elsevier, 2012, vol. 504, pp. 109–125.
17 J. R. Conway, N. O. Carragher and P. Timpson, *Nat. Rev. Cancer*, 2014, **14**, 314–328.
18 Y. Ardeshirpour, V. Chernomordik, M. Hassan, R. Zielinski, J. Capala and A. Gandjbakhche, *Clin. Cancer Res.*, 2014, **20**, 3531–3539.
19 P. Manna, S.-T. Hung, S. Mukherjee, P. Friis, D. M. Simpson, M. N. Lo, A. E. Palmer and R. Jimenez, *Integr. Biol.*, 2018, **10**, 516–526.
20 A. V. Gohar, R. Cao, P. Jenkins, W. Li, J. P. Houston and K. D. Houston, *Biomed. Opt. Express*, 2013, **4**, 1390–1400.
21 J. Sambrano, A. Chigaev, K. S. Nichani, Y. Smagley, L. A. Sklar and J. P. Houston, *J. Biomed. Opt.*, 2018, **23**, 075004.

 

22 M. Suzuki, I. Sakata, T. Sakai, H. Tomioka, K. Nishigaki, M. Tramier and M. Coppey-Moisan, *Anal. Biochem.*, 2015, **491**, 10–17.
23 F. Alturkistany, K. Nichani, K. D. Houston and J. P. Houston, *Cytometry, Part A*, 2019, **95**, 70–79.
24 W. Li, K. D. Houston and J. P. Houston, *Sci. Rep.*, 2017, **7**, 40341.
25 B. Sands, P. Jenkins, W. J. Peria, M. Naivar, J. P. Houston and R. Brent, *PLoS One*, 2014, **9**, e109940.
26 A. I. Skilitsi, T. Turko, D. Cianfarani, S. Barre, W. Uhring, U. Hassiepen and J. Léonard, *Methods Appl. Fluoresc.*, 2017, **5**, 034002.
27 J.-C. Baret, O. J. Miller, V. Taly, M. Ryckelynck, A. El-Harrak, L. Frenz, C. Rick, M. L. Samuels, J. B. Hutchison and J. J. Agresti, others, *Lab Chip*, 2009, **9**, 1850–1858.
28 A. Fallah-Araghi, J.-C. Baret, M. Ryckelynck and A. D. Griffiths, *Lab Chip*, 2012, **12**, 882–891.
29 L. Mazutis, J. Gilbert, W. L. Ung, D. A. Weitz, A. D. Griffiths and J. A. Heyman, *Nat. Protoc.*, 2013, **8**, 870–891.
30 K. Churski, T. S. Kaminski, S. Jakiela, W. Kamysz, W. Baranska-Rybak, D. B. Weibel and P. Garstecki, *Lab Chip*, 2012, **12**, 1629–1637.
31 X. Liu, R. Painter, K. Enesa, D. Holmes, G. Whyte, C. Garlisi, F. Monsma, M. Rehak, F. Craig and C. A. Smith, *Lab Chip*, 2016, **16**, 1636–1643.
32 B. Kintses, C. Hein, M. F. Mohamed, M. Fischlechner, F. Courtois, C. Lainé and F. Hollfelder, *Chem. Biol.*, 2012, **19**, 1001–1009.
33 Y. Zhao, A. S. Abdelfattah, Y. Zhao, A. Ruangkittisakul, K. Ballanyi, R. E. Campbell and D. J. Harrison, *Integr. Biol.*, 2014, **6**, 714–725.
34 B. L. Fiedler, S. Van Buskirk, K. P. Carter, Y. Qin, M. C. Carpenter, A. E. Palmer and R. Jimenez, *Anal. Chem.*, 2016, **89**, 711–719.
35 E. Papalexi and R. Satija, *Nat. Rev. Immunol.*, 2018, **18**, 35–45.
36 V. Chokkalingam, J. Tel, F. Wimmers, X. Liu, S. Semenov, J. Thiele, C. G. Figdor and W. T. Huck, *Lab Chip*, 2013, **13**, 4740–4744.
37 S. Moon, E. Ceyhan, U. A. Gurkan and U. Demirci, *PLoS One*, 2011, **6**, e21580.
38 D. J. Collins, A. Neild, A. DeMello, A.-Q. Liu and Y. Ai, *Lab Chip*, 2015, **15**, 3439–3459.
39 A. Sciambi and A. R. Abate, *Lab Chip*, 2015, **15**, 47–51.
40 S. Hasan, D. Geissler, K. Wink, A. Hagen, J. J. Heiland and D. Belder, *Lab Chip*, 2019, **19**, 403–409.
41 T.-J. Wu, Y.-K. Tzeng, W.-W. Chang, C.-A. Cheng, Y. Kuo, C.-H. Chien, H.-C. Chang and J. Yu, *Nat. Nanotechnol.*, 2013, **8**, 682.
42 D. Lando, S. Basu, T. J. Stevens, A. Riddell, K. J. Wohlfahrt, Y. Cao, W. Boucher, M. Leeb, L. P. Atkinson and S. F. Lee, others, *Nat. Protoc.*, 2018, **13**, 1034–1061.
43 E. Braselmann, A. J. Wierzba, J. T. Polaski, M. Chromiński, Z. E. Holmes, S.-T. Hung, D. Batan, J. R. Wheeler, R. Parker and R. Jimenez, others, *Nat. Chem. Biol.*, 2018, **14**, 964–971.
44 D.-K. Kang, M. M. Ali, K. Zhang, S. S. Huang, E. Peterson, M. A. Digman, E. Gratton and W. Zhao, *Nat. Commun.*, 2014, **5**, 5427.
45 C.-Y. Ou, T. Vu, J. T. Grunwald, M. Toledano, J. Zimak, M. Toosky, B. Shen, J. A. Zell, E. Gratton and T. J. Abram, others, *Lab Chip*, 2019, **19**, 993–1005.
46 P. N. Hedde, T. Abram, T. Vu, W. Zhao and E. Gratton, *Biomed. Opt. Express*, 2019, **10**, 1223–1233.
47 R. Turk-MacLeod, A. Henson, M. Rodriguez-Garcia, G. M. Gibson, G. A. Camarasa, D. Caramelli, M. J. Padgett and L. Cronin, *Proc. Natl. Acad. Sci. U. S. A.*, 2018, **115**, 5681–5685.
48 J. Myung and S. Hong, *Lab Chip*, 2015, **15**, 4500–4511.
49 T. Lieske, W. Uhring, N. Dumas, A. I. Skilitski, J. Léonard and D. Fey, *J. Signal Process Syst.*, 2019, **91**, 819–831.
50 Y. Shen, Y. Chen, J. Wu, N. C. Shaner and R. E. Campbell, *PLoS One*, 2017, **12**, e0171257.
51 P. Manna and R. Jimenez, *J. Phys. Chem. B*, 2015, **119**, 4944–4954.
52 Y. Nov, *Appl. Environ. Microbiol.*, 2012, **78**, 258–262.
53 K. S. Sarkisyan, D. A. Bolotin, M. V. Meer, D. R. Usmanova, A. S. Mishin, G. V. Sharonov, D. N. Ivankov, N. G. Bozhanova, M. S. Baranov and O. Soylemez, others, *Nature*, 2016, **533**, 397–401.